Received: 28 August 2019 | Revised: 18 October 2019 | Accepted: 21 October 2019 | Published on: 9 December 2019

DOI: 10.1002/ctpp.201900117



ORIGINAL ARTICLE

Contributions to Plasma Physics

# Collisional gyrokinetic full-f particle-in-cell simulations on open field lines with PICLS

**Mathias Boesl**[1] | **Andreas Bergmann**[1] | **Alberto Bottino**[1] | **Stephan Brunner**[2] | **David Coster**[1] | **Frank Jenko**[1]

[1]Max Planck Institut für Plasmaphysik, Garching, Germany

[2]Swiss Plasma Center, Ecole Polytechnique Fédérale de Lausanne, Lausanne, Switzerland

**Correspondence**
Mathias Boesl, Max Planck Institut für Plasmaphysik, D-85748 Garching, Germany.
Email: mathias.boesl@ipp.mpg.de

**Present Address**
Mathias Boesl, Boltzmannstrasse 2, 85748 Garching, Germany.

**Funding information**
H2020 Euratom, 633053

**Abstract**

Applying gyrokinetic simulations in theoretical turbulence and transport studies for the plasma edge and scrape-off layer (SOL) presents significant challenges. To particularly account for steep density and temperature gradients in the SOL, the "full-f" code PICLS was developed. PICLS is a gyrokinetic particle-in-cell (PIC) code, is based on an electrostatic model with a linearized field equation, and uses kinetic electrons. In previously published results, we applied PICLS to the well-studied 1D parallel transport problem during an edge-localized mode (ELM) in the SOL without collisions. As an extension to this collision-less case and in preparation for 3D simulations, in this work, a collisional model will be introduced. The implemented Lenard–Bernstein collision operator and its Langevin discretization will be shown. Conservation properties of the collision operator, as well as a comparison of the collisional and non-collisional case, will be discussed.

**KEYWORDS**

collisions, gyrokinetics, particle-in-cell, scrape-off layer, turbulence

## 1 | INTRODUCTION

In the closed field line region of the plasma core, gyrokinetics has become the workhorse for turbulence simulations in the last decades, but their extension towards the plasma edge and scrape-off layer (SOL) demonstrates additional challenges. Therefore, in a previous work,[1] we investigated the well-studied problem of parallel energy and particle transport caused by a transient Type I edge-localized mode (ELM) in the SOL. Heat pulse simulations with a single central source model were already studied with fully kinetic particle-in-cell (PIC), continuum (Vlasov), and fluid codes and successfully benchmarked against the experiment.[2] Therefore, in our previous work, we also studied this problem and achieved good agreement with very recent gyrokinetic continuum code simulations[3–5] in the collision-less case that reproduced the results of the mentioned previous works.[2]

However, collisions are a key driver to transport particles across closed magnetic flux surfaces that would be otherwise confined.[6] They cause plasma to diffuse from the confined region into the SOL, and from there, they are transported towards the device wall.[6] Due to lower temperature, collisionality is also higher in the SOL than in the core region.

Therefore, in this study, we implement a Lenard–Bernstein (LB) collision operator in our newly developed PICLS code, which is designed to perform gyrokinetic SOL simulations.[1] For the applied PIC model, the operator is discretized via a Langevin approach.[7] We will show that the implemented LB collision operator conserves particle number, parallel momentum, and energy and relaxes towards a Maxwellian. In addition, we will repeat our previously studied one spatial 1 velocity domain (1D1V) heat pulse problem in a modified one spatial 2 velocity domains (1D2V) version—with the magnetic moment $\mu$ as an additional coordinate—and compare the collision-less with the collisional case.

The electrostatic gyrokinetic equations implemented in PICLS for the 1D heat pulse problem are described in Section 2. In Section 3, the considered LB collision operator and its PIC discretization is introduced. Simulation results for collision operator testing and the 1D2V collisional heat pulse problem are shown in Sections 4 and 5. Section 6 contains conclusions and an outlook.

## 2 | PHYSICAL MODEL

The equations implemented in PICLS are derived from a low-frequency and electrostatic gyrokinetic model with kinetic electrons. Due to the 1D ELM pulse problem investigated here, finite-Larmor radius (FLR) effects are not required. However, Larmor radius effects and gyroaveraging are already implemented for future higher-dimensional simulations. As of now, PICLS is purely based on slab geometry, and for the 1D heat pulse problem, only the 1D slab versions of the Euler–Lagrange eqs. for position $z$ and parallel velocity $v_\parallel$ are required. By choosing $B =$ const and parallel to the $z$-direction, for species $p$, these can be written as:

$$\dot{z} = v_\parallel \mathbf{b}, \qquad \dot{v_\parallel} = -\frac{e_p}{m_p}\mathbf{b}\cdot\nabla J_{p,0}\phi \tag{1}$$

with the gyroaveraging operator $J_{p,0}$. By introducing the shielding factor $s_\perp(z,t) = k_\perp^2(z)\varepsilon_\perp(z,t)$, with $\varepsilon_\perp = \sum_p \frac{n_{p,0}m_p c^2}{B^2}$, a simplified polarization equation can be obtained that only takes a single perpendicular wave number $k_\perp$ into account[4,5]:

$$s_\perp(z,t)(\phi - \langle\phi\rangle) = \sum_p \int \mathrm{d}W e_p J_{p,0} f, \tag{2}$$

where the flux surface-averaged, dielectric-weighted potential $\langle\phi\rangle = \frac{\int dz s_\perp \phi}{\int dz s_\perp}$ is used. For more details on the derivation of the physical model and its numerical discretization, we refer to our previously published work.[1]

A logical sheath model is implemented to model the effects of a Debye sheath without actually having to resolve it. The setup of the implemented logical sheath is generally based on the model shown in Parker et al.,[8] which was developed for fully kinetic 1D2V PIC simulations. The same model was used for previous parallel heat flux studies with gyrokinetic 1D1V continuum codes.[3,5] Here, the total parallel current $j_\parallel$ to the wall is set to 0. This model mimics the physical effect of accelerating incident ions by the decreasing sheath potential $\phi_{\mathrm{sh}}$. For electrons, however, the velocity needs to be high enough to overcome the $\phi_{\mathrm{sh}}$ drop at the boundary, and slower electrons are reflected backwards. With the wall potential $\phi_{\mathrm{w}}$ ($\phi_{\mathrm{w}} = 0$ for a grounded wall), the electron cut-off velocity $v_{\mathrm{ce}}$, which is the velocity of the slowest electron exiting the domain, determines $\phi_{\mathrm{sh}}$ according to:

$$\delta\phi = \phi_{\mathrm{sh}} - \phi_{\mathrm{w}} = \frac{m}{2e}v_{\mathrm{ce}}^2. \tag{3}$$

As already described in our previous work,[1] the $j_\parallel = 0$ condition at the sheath position $z_{\mathrm{sh}}$ can be expressed as:

$$\Sigma_{\mathrm{i}} q_{\mathrm{i}} \int_0^\infty f_{\mathrm{i}}(z_{\mathrm{sh}}, v_\parallel, t) v_\parallel dv_\parallel = e\int_{v_{\mathrm{ce}}}^\infty f_{\mathrm{e}}(z_{\mathrm{sh}}, v_\parallel, t) v_\parallel dv_\parallel, \tag{4}$$

with $f_{\mathrm{e}}$ being the electron and $f_{\mathrm{i}}$ being the ion distribution function. For $f_{\mathrm{e}}$ and $f_{\mathrm{i}}$ at the wall, due to the total absorption of ions and the partial absorption of electrons at $z_{\mathrm{sh}}$, we obtain:

$$f_{\mathrm{i}}(z_{\mathrm{sh}}, -v_\parallel, t) = 0 \qquad v_\parallel > 0 \tag{5}$$

$$f_{\mathrm{e}}(z_{\mathrm{sh}}, -v_\parallel, t) = \begin{cases} 0 & v_\parallel > v_{\mathrm{ce}} \\ f_{\mathrm{e}}(z_{\mathrm{sh}}, v_\parallel, t) & v_{\mathrm{ce}} > v_\parallel > 0. \end{cases} \tag{6}$$

The equations are formulated for a sheath on the right side of the domain, with $v_\parallel$ going into the wall (similar for left side).

## 3 | LB COLLISION OPERATOR

To account for collisions in our model, the LB collision operator is implemented.[9,10] It can be used in the presence of small-angle collisions and includes collision-driven diffusion in velocity space, which causes the distribution function to relax towards a Maxwellian. The results of a Landau operator are recovered in the limit of infrequent collisions.[9] However, in the simplified LB operator, the evaluation of Rosenbluth potentials is avoided. The operator contains pitch-angle scattering and conserves particle number, momentum, and energy analytically. It assumes long wavelength, that is, ignores FLR corrections. The LB collision operator acting on the full-f model for species $p$ and $p'$ is written as:

$$\begin{aligned} C_p[f_p] &= \sum_{p'} C_{pp'}[f_p] = \sum_{p'} \nu_{pp'} \frac{\partial}{\partial \mathbf{v}} \cdot \left[ (\mathbf{v} - \mathbf{u}_{\parallel,\mathbf{p}'}) f_p + v_{T,pp'}^2 \frac{\partial f_p}{\partial \mathbf{v}} \right] \\ &= \sum_{p'} \nu_{pp'} \left( \frac{\partial}{\partial v_\parallel} \left[ (v_\parallel - u_{\parallel,p'}) f_p + v_{T,pp'}^2 \frac{\partial f_p}{\partial v_\parallel} \right] + \frac{\partial}{\partial \mu} \left[ 2\mu f_p + 2 \frac{m_p v_{T,pp'}^2}{B} \mu \frac{\partial f_p}{\partial \mu} \right] \right) \end{aligned} \tag{7}$$

with the definitions:

$$u_\parallel = \frac{\int d^3v v_\parallel f_p}{n_p} \tag{8}$$

$$m_p v_{T,pp'}^2 = \frac{\int d^3v m_p (\mathbf{v} - \mathbf{u}_{\mathbf{p}'})^2 f_p}{3 n_p} \tag{9}$$

$$n_p = \int d^3v f_p. \tag{10}$$

In addition, for the collision frequencies of self-species collisions, standard expressions can be used that are defined as $\nu_{ee} = \frac{4\sqrt{2\pi} n_e \lambda e^4}{3\sqrt{m_e} T_e^{3/2}}$ and $\nu_{ii} = \frac{4\sqrt{\pi} n_i \lambda e^4}{3\sqrt{m_i} T_i^{3/2}}$. Here, $\lambda$ stands for the Coulomb logarithm $\lambda = 6.6 - 0.5 \ln(n_0/10^{20}) + 1.5 \ln T_{e0}$, where $n_0$ is expressed in $m^{-3}$ and $T_{e0}$ in eV. For electron–ion collisions, the LB collision operator is also used for simplicity with the collision frequency $\nu_{ei} = \nu_{ee}/1.96$, which approximately accounts for the plasma's parallel conductivity coefficient. Ion–electron collisions are neglected as $\nu_{ie}$ is much smaller than the ion–ion term ($\nu_{ie}/\nu_{ii} \sim \sqrt{m_e/m_i}$), as also used in gyrokinetic continuum code studies in Gkeyll and GENE.[11,12] The drag coefficient $\Gamma$ and diffusion coefficient $D$ can be extracted from Equation (7):

$$\Gamma = -\nu_{pp'}(\mathbf{v} - \mathbf{u}_{\parallel,\mathbf{p}'}), \qquad D = \nu_{pp'} v_{T,pp'}^2. \tag{11}$$

To discretize the LB collision operator for our PIC approach, we use the so-called Langevin approach as explained in Vernay et al.[7] Applying this approach, the position in phase space $x_n(t)$ of marker $n$ at time $t$ is given by its previous position $x_n(t - \Delta t)$ at time step $t - \Delta t$ according to:

$$\Delta x_n = x_n(t) - x_n(t - \Delta t) = \langle \Delta x \rangle + \mathcal{R} \sqrt{\langle \Delta x \Delta x \rangle} = \Gamma \Delta t + \mathcal{R} \sqrt{2D \Delta t}, \tag{12}$$

where $\mathcal{R}$ is a random number sampled from a probability distribution function (PDF) of average 0 and variance 1. To ensure that $\xi_{out} = v_\parallel / v \in [-1, 1]$, one temporarily expands the 2D gyrokinetic velocity space to 3D.[7] Using the drag and diffusion coefficients (11) in (12), we achieve the velocity change in the $(v_x, v_y, v_z)$ space, where $v_z$ is along $v_\parallel$, and $v_x$ and $v_y$ can be freely chosen in the plane perpendicular to $v_\parallel$ (we chose $v_x$ along $v_{\perp,in}$):

$$\Delta v_x = -\nu_{pp'} v_{\perp,in} \Delta t + v_{T,pp'} \sqrt{2\nu_{pp'} \Delta t} \mathcal{R}_1, \quad \Delta v_y = v_{T,pp'} \sqrt{2\nu_{pp'} \Delta t} \mathcal{R}_2, \quad \Delta v_z = -\nu_{pp'}(v_{\parallel,\mathrm{in}} - u_{\parallel,p'}) \Delta t + v_{T,pp'} \sqrt{2\nu_{pp'} \Delta t} \mathcal{R}_3, \tag{13}$$

with $v_\perp = \sqrt{2B(\mathbf{R})\ \mu/\mathrm{m}}$ and the independent random numbers $\mathcal{R}_1$, $\mathcal{R}_2$, and $\mathcal{R}_3$. To achieve the velocity values for the outgoing marker after the collision operation, one has to reverse-transform the coordinates back to the 2D velocity space:

$$v_{\parallel,\mathrm{out}} = v_{\parallel,\mathrm{in}} + \Delta v_z, \qquad v_{\perp,\mathrm{out}} = \sqrt{(v_{\perp,\mathrm{in}} + \Delta v_x)^2 + \Delta v_y^2}. \tag{14}$$

For the collision operator implementation, conservation of particle number, parallel momentum $\sim\langle v_\parallel\rangle$, and kinetic energy $\sim\langle v^2\rangle$ is decisive. Analytically, the LB operator conserves these quantities for infinitely small time steps and an infinite number of particles. However, for finite values of both, the time step, and the particle number, corrections can be introduced to ensure that conservation relations hold up to round-off (machine precision). In PICLS, for simplicity, we have only implemented such a correction to account for the finite time step $\Delta t$ but not to account for statistical errors related to finite number of particles. For our use, these corrections already show good conservation of moments as presented in Section 4. As PICLS is based on a full-f model, particle number is intrinsically conserved. For $\langle v_\parallel\rangle$ and $\langle v^2\rangle$, the idea, however, is to regard $u_\parallel$ and $v_T$ as free parameters, which are determined in order to ensure the conservation of moments. For the parallel momentum, we set the change of the average parallel velocity to zero, which corresponds to $\Delta v_z$ from Equation (13), as $v_\parallel$ lies in the $z$-direction. We sum all marker weights within a configuration space bin to achieve:

$$0=\sum_{n=1}^{N} w_n \Delta v_{\parallel,n}=\sum_{n=1}^{N} w_n \Delta v_{z,n}=\sum_{n=1}^{N} w_n[-\nu(v_{\parallel,in,n}-u_\parallel)\Delta t+v_T\sqrt{2\nu\Delta t}\mathcal{R}_{3,n}], \tag{15}$$

with $N$ being the total number of markers within the bin. Using the relation $\langle\mathcal{R}_{3,n}\rangle=0$, which is a result of our choice of the PDF, the second term drops, and we can achieve a relation for $\langle u_\parallel\rangle$ to conserve parallel momentum:

$$\langle u_\parallel\rangle=\sum_{n=1}^{N} w_n v_{\parallel,in,n}/\sum_{n=1}^{N} w_n, \tag{16}$$

which is exactly the obvious PIC discretization relation for (8). Thus, no correction for $u_\parallel$ is required to conserve parallel momentum. The next step is to derive a relation for $v_T$ in order to conserve energy. For this, the derived relation for $u_\parallel$ (16) can be used. On average, over all particles, the following relation for the total change of kinetic energy must hold:

$$0=\mathbf{v}_{\text{out}}^2-\mathbf{v}_{\text{in}}^2=(\mathbf{v}+\Delta\mathbf{v})^2-\mathbf{v}^2=2\mathbf{v}\Delta\mathbf{v}+(\Delta\mathbf{v})^2. \tag{17}$$

Writing the explicit expression for $\Delta\mathbf{v}$ that follows from Equation (12) with $\vec{\mathcal{R}}=(\mathcal{R}_1,\mathcal{R}_2,\mathcal{R}_3)$ and summing the markers yields:

$$0=\sum_{n=1}^{N} w_n\{2(\mathbf{v}_{\text{in},n}-\mathbf{e}_z u_\parallel)\cdot[-\nu\Delta t(\mathbf{v}_{\text{in},n}-\mathbf{e}_z u_\parallel)+v_T\sqrt{2\nu\Delta t}\vec{\mathcal{R}}_n]+[-\nu\Delta t(\mathbf{v}_{\text{in},n}-\mathbf{e}_z u_\parallel)+v_T\sqrt{2\nu\Delta t}\vec{\mathcal{R}}_n]^2\} \tag{18}$$

$$=\sum_{n=1}^{N} w_n\{-\nu\Delta t(2-\nu\Delta t)(\mathbf{v}_{\text{in},n}-\mathbf{e}_z u_\parallel)^2+2v_T\sqrt{2\nu\Delta t}(1-\nu\Delta t)(\mathbf{v}_{\text{in},n}-\mathbf{e}_z u_\parallel)\mathcal{R}_n+2v_T^2\nu\Delta t\vec{\mathcal{R}}_n^2\}. \tag{19}$$

Invoking the properties of the PDF for the random numbers $\langle\vec{\mathcal{R}}_n\rangle=0$ and $\langle\vec{\mathcal{R}}_n^2\rangle=\langle\mathcal{R}_{1,n}^2\rangle+\langle\mathcal{R}_{2,n}^2\rangle+\langle\mathcal{R}_{3,n}^2\rangle=3$, one obtains:

$$3\left(\sum_{n=1}^{N} w_n\right)2\nu\Delta t\langle v_T^2\rangle=\nu\Delta t(2-\nu\Delta t)\sum_{n=1}^{N} w_n(\mathbf{v}_{\text{in},n}-\mathbf{e}_z u_\parallel)^2. \tag{20}$$

A relation for $\langle v_T^2\rangle$ to conserve kinetic energy can directly be derived from Equation (20):

$$\langle v_T^2\rangle=(1-\nu\Delta t/2)\frac{\sum_{n=1}^{N} w_n(\mathbf{v}_{\text{in},n}-\mathbf{e}_z u_\parallel)^2}{3\sum_{n=1}^{N} w_n}. \tag{21}$$

This relation appears to be the appropriate PIC discretization of (9). Note the correction factor $(1-\nu\Delta t/2)$, which is required to achieve conservation of kinetic energy for finite time steps.

## 4 | SIMULATION RESULTS: 1D2V COLLISION OPERATOR TESTING

To decrease complexity and test against analytic functions, we choose a single species $p$ subject to self-species collisions and set $\mathbf{u}_\parallel=0$, $v_T=\text{const}$ and $\nu=\text{const}$. With this setting, the evolution eq. for the distribution $f$ is given by:

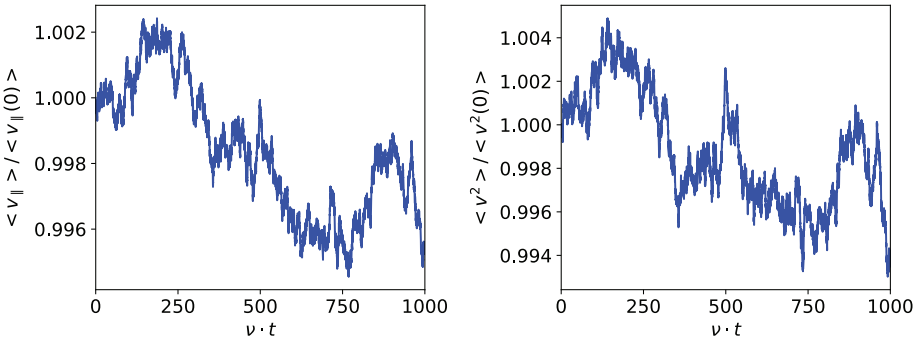


**FIGURE 1** Time evolution of $\langle v_\parallel(t)\rangle/\langle v_\parallel(0)\rangle$ and $\langle v(t)^2\rangle/\langle v(0)^2\rangle$ for simulations with self-consistent calculation of $\mathbf{u}_\parallel$ and $v_T$ and 100,000 particles per cell plotted for a total simulation time (in $\nu \cdot t$). Parallel momentum and kinetic energy are mostly conserved with ~1% deviation from initial values.

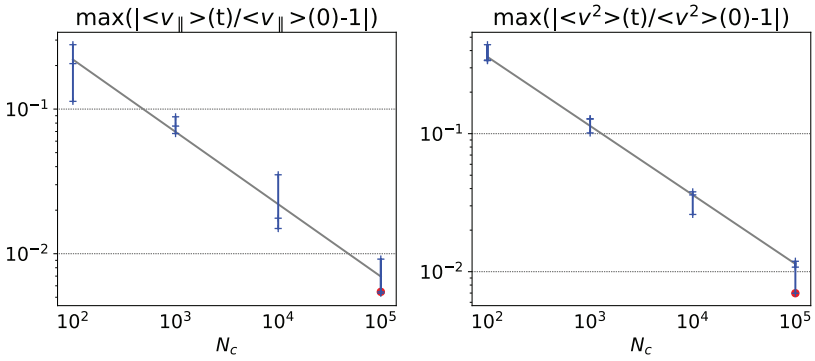


**FIGURE 2** Convergence of the conservation error for $\langle v_\parallel\rangle$ and $\langle v^2\rangle$ with varying number of markers per cell ($N_c$). Each blue cross coincides with a conservation study similar to Figure 1 for a specific $N_c$ and a random initialization of markers (the data point of Figure 1 is indicated in red). The convergence in both cases is $\propto 1/\sqrt{N_c}$ (indicated by the grey line).

$$\frac{\partial}{\partial t} f = C_p[f] = \nu \frac{\partial}{\partial \mathbf{v}} \cdot \left[ \mathbf{v} f + v_T^2 \frac{\partial f}{\partial \mathbf{v}} \right]. \tag{22}$$

With the definitions for density $n = \int d^3v f$, average velocity $\langle \mathbf{v} \rangle = \int d^3v \mathbf{v} f/n$, and kinetic energy $\langle v^2 \rangle = \int d^3v v^2 f/n$, analytic expressions can be derived for the time evolution of these quantities and compared with the numerical simulations. For $\langle \mathbf{v} \rangle$ and $\langle v^2 \rangle$, the following exponentially decaying functions can be found as solutions:

$$\langle \mathbf{v} \rangle(t) = \langle \mathbf{v} \rangle(t=0) e^{-\nu t}, \qquad \langle v^2 \rangle(t) = 3v_T^2 + [\langle v^2 \rangle(t=0) - 3v_T^2] e^{-2\nu t}. \tag{23}$$

By choosing an arbitrary initial velocity distribution, which has to relax according to Equation (23), we can construct the first test case for the implemented collision operator. Performing this test case demonstrates that the implemented operator is able to reproduce the analytic results of Equation (23), and the marker distribution relaxes to a Maxwellian with the considered values for $\mathbf{u}_\parallel$ and $v_T$ in the equilibrated state.

As a second test case, the more general form of the collision operator, as in (3), is considered, which calculates $\mathbf{u}_\parallel$ and $v_T$ at each time step according to (16) and (21). Here, the previously mentioned correction factor $(1 - \nu\Delta t/2)$ for estimating $v_T$ is implemented. For conservation tests, single species, and thus only self-species, collisions are used. An arbitrary initial particle distribution should relax towards a Maxwellian in $v_\parallel$ and conserve $\langle \mathbf{v} \rangle$ and $\langle v^2 \rangle$. The number of particles is automatically conserved due to the chosen full-f model. Figure 1 shows the time evolution of $\langle v_\parallel(t)\rangle/\langle v_\parallel(0)\rangle$ and $\langle v(0)^2\rangle/\langle v(0)^2\rangle$ for an exemplary simulation to highlight the changes of parallel momentum and kinetic energy. Despite choosing a marker number per bin (of 100, 000) that is ≥3 times lower than those of the 1D heat pulse simulations in Section 5, in Figure 1, $\langle v_\parallel \rangle$ and $\langle v^2 \rangle$ are mostly conserved with only a variation of <2% in its initial value. In Figure 2, the convergence of the conservation error for $\langle v_\parallel \rangle$ and $\langle v^2 \rangle$ is shown. By increasing the number of markers, the deviations decrease and follow a $1/\sqrt{N_c}$ dependence, with $N_c$ being the number of markers per cell. Again, an arbitrary initial marker distribution in $v_\parallel$ relaxes to a Maxwellian, but this time, its maximum remains at the initialized $\mathbf{u}_\parallel$. As the parallel momentum conservation property holds, the particle velocities remain distributed around their initial $\mathbf{u}_\parallel$.

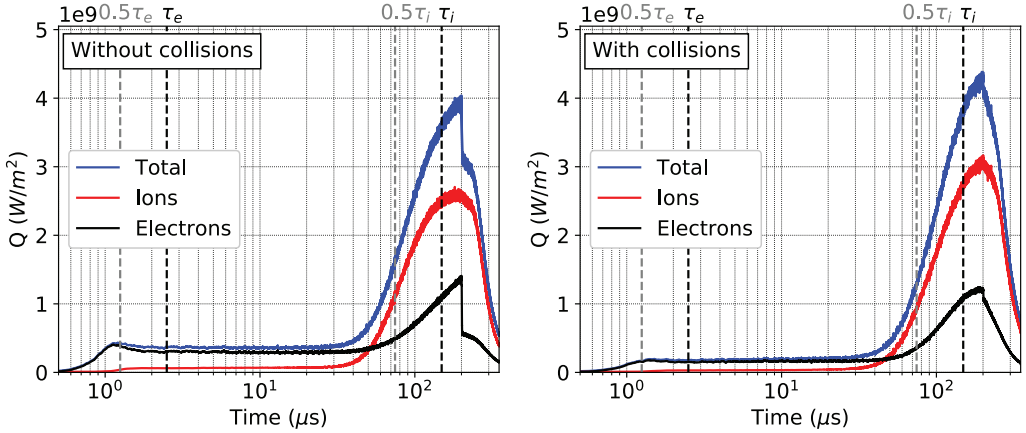


**FIGURE 3** Comparison of the evolution of ion (red), electron (black), and total (blue) heat flux in the 1D2V case, according to Equation (24), with and without same-species Lenard–Bernstein collisions. Thermal ion and electron transit times $\tau_e = 2.5$ μs and $\tau_i = 149$ μs are indicated by black vertical lines ($0.5\tau_e$ and $0.5\tau_i$ are indicated by grey lines).

## 5 | SIMULATION RESULTS: COLLISIONAL 1D2V HEAT PULSE

In our previous publication,[1] we performed simulations on a 1D heat pulse in the SOL without collisions. There, a high-energy particle source acted as an ELM heat pulse and injected particles for 200 μs. Within this work, we again want to use the same setup. However, in view of realistic SOL simulations, particle collisions are introduced. We therefore introduce the magnetic moment $\mu$ as a second velocity component and use the LB collision operator, described in Section 3. Inter-species collisions between electrons and ions are neglected similar to the work conducted by Shi et al.[3]

By introducing $\mu$, the fixed $T_\perp$ from our previous work[1] now can also be changed over time by the collision operator. For the heat pulse source, the perpendicular temperature, however, is kept constant at $T_{\text{ped}}$, even after the ELM heat pulse ends. For the parallel temperature, the same setup as described in Boesl et al.[1] will be used. With $\mu$ as an additional velocity component, the equation for the parallel heat flux can be written as:

$$Q_p = \int_{v_{c,p}}^{\infty} f_p v_\parallel \left(\frac{1}{2} m_p v_\parallel^2 + \mu B\right) dv_\parallel + q_p \phi_{\text{sh}} \int_{v_{c,p}}^{\infty} f_p v_\parallel dv_\parallel. \tag{24}$$

For the simulations within this section, the initial marker distribution was initiated with ∼300,000 markers per bin, which is three times higher than in the presented conversion study in Figure 1 in Section 4. Thus, we can ensure that the conservation error is small enough. The total number of markers even increases once the particle sources introduce particles into the simulation domain. This high number of markers per cell is excessive, but as the simulations can be run within hours, we did not want to allow an increase of the noise by lowering the marker number. Figure 3 compares the heat flux on the divertor wall for non-collisional and collisional 1D2V simulations. We want to emphasize that the values in the 1D2V collision-less case differ from the 1D1V simulations of our previous work[1] due to the source applied for the $\mu$ initialization. The first differences we notice between both plots is a lower initial heat flux before $\sim 0.5\tau_i$ for the collisional case, which is about 50% of the non-collisional case. Once the supra-thermal ions hit the wall, the ion heat flux in the collisional case rises even higher than in the non-collisional case. However, for the electrons, a slight decrease in the maximum heat flux is visible. For the total heat flux, ∼8% higher maximal value ($4.04 \times 10^9$ W/m$^2$ vs. $4.38 \times 10^9$ W/m$^2$) is thus reached in the collisional case. Investigating the heat flux in the collisional (non-collisional) case further demonstrates more differences. The share of the total heat flux over time deposited before the peak at 200 μs is 55% (61%), and for the total heat flux deposited by ions versus electrons, we obtain shares of 74% versus 26% (72% vs. 28%). The total heat flux deposited over time in the collisional case is 9% higher than in the non-collisional case. This clearly shows that the collisions introduced lead to an increase in the ion heat flux and, over time, lead to a higher heat flux on the wall. This largely depends on the increased particle flux, but to better understand the heat flux evolution, in Figure 4, a comparison of the sheath potential $\phi_{\text{sh}}$ with and without collisions is shown. First, $\phi_{\text{sh}}$ in both cases is determined by the cold initial distribution. However, at ∼0.5–1 $\tau_e$, both curves increase rapidly due to arriving supra-thermal electrons from the ELM source. In the collision-less case, $\phi_{\text{sh}}$ immediately rises to ∼3 keV, where it stays mainly constant until the arrival of supra-thermal

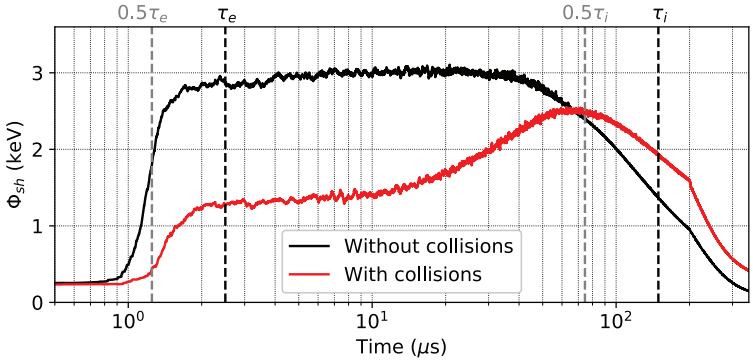


**FIGURE 4** Comparison of the time-dependent evolution of the sheath potential at the right boundary in the 1D2V case with and without same-species Lenard–Bernstein collisions. The vertical black and grey lines are at the same position as in Figure 3.

ions at $\sim 0.5\tau_i$. On the other hand, in the collisional case, $\phi_{sh}$ rises quickly to ~1.5 keV and then gradually increases up to its maximum of ~2.5 keV at $\tau_i$. This is an indicator that the collision operator decreases the high-$v_\parallel$ tail of the velocity distribution as a result of drag on ions or thermalization through self-collisions. In both cases, the $\phi_{sh}$ decelerates and reflects electrons at the wall. The majority of electrons are prevented from leaving the domain, and thus, the increase of the electron flux is stopped at $\sim 0.5\tau_e$. The sheath potential decreases steadily after the inflow of supra-thermal ions and allows an increase of both the ion and electron flux. However, $\phi_{sh}$ remains higher for the collisional case after $\sim 0.5\tau_i$. This again can be described by the collision operator, which is able to replenish high-$v_\parallel$ electrons through pitch-angle scattering.

## 6 | CONCLUSIONS

Different from our previous publication,[1] in the current work, an LB collision operator for same-species collisions was implemented in the gyrokinetic PIC code PICLS. The operator's PIC discretization and conservation properties were discussed, and a correction term to conserve energy up to round-off (machine precision) for finite time steps and an infinite number of particles was derived. Using this correction for a finite number of particles, very good energy conservation could still be shown. Following our previous work,[1] with the new collisional model, 1D2V heat pulse simulations were performed and compared with non-collisional results. Collisions had a significant effect on the heat flux deposited on the sheath, which increases by a total of 9%. The sheath potential $\phi_{sh}$ also demonstrates a deferred increase and lower maximum of ~2.5 keV (compared to ~3.0 keV) due to collisional effects. Implementing a working collisional model, PICLS can now be extended to a higher spatial dimension for future simulations.

## ACKNOWLEDGMENTS

The authors thank L. Villard, N. Ohana, and E. Lanti from the Swiss Plasma Center (Lausanne) for their help. Numerical simulations were performed on the Marconi supercomputer within the framework of the PICLS project. This work has also been carried out within the framework of the EUROfusion Consortium and has received funding from the Euratom research & training program 2014–2018 and 2019–2020 under grant agreement No. 633053, for the EF WP32-ENR-MPG-04 (2019/2020) project "MAGYK." The views and opinions expressed here do not necessarily reflect those of the European Commission.

## REFERENCES

[1] M. Boesl, A. Bergmann, A. Bottino, D. Coster, E. Lanti, N. Ohana, F. Jenko, *arXiv preprint arXiv*:1908.00318, **2019**.
[2] E. Havlíčková, W. Fundamenski, D. Tskhakaya, G. Manfredi, D. Moulton, *Plasma Phys. Controlled Fusion* **2012**, *54*, 045002.
[3] E. L. Shi, A. H. Hakim, G. W. Hammett, *Phys. Plasmas* **2015**, *22*, 022504.
[4] E. L. Shi, *arXiv preprint arXiv:1708.07283*, **2017**.
[5] Q. Pan, D. Told, F. Jenko, *Phys. Plasmas* **2016**, *23*, 102302.
[6] P. Ricci, *J. Plasma Phys.* **2015**, *81*, 435810202.
[7] T. Vernay, *Collisions in Global Gyrokinetic Simulations of Tokamak Plasmas using the Delta-f Particle-In-Cell Approach*, EPFL, Lausanne, **2013**.
[8] S. E. Parker, R. J. Procassini, C. K. Birdsall, B. I. Cohen, *J. Comput. Phys.* **1993**, *104*(1), 41.
[9] A. Lenard, I. B. Bernstein, *Phys. Rev.* **1958**, *112*, 1456.

[10] J. P. Dougherty, *Phys. Fluids* **1964**, *7*, 1788.
[11] E. L. Shi, G. W. Hammett, T. Stoltzfus-Dueck, A. Hakim, *J. Plasma Phys.* **2017**, *83*(3), 905830304.
[12] Q. Pan, D. Told, E. L. Shi, G. W. Hammett, F. Jenko, *Phys. Plasmas* **2018**, *25*, 062303.

**How to cite this article:** Boesl M, Bergmann A, Bottino A, Brunner S, Coster D, Jenko F. Collisional gyrokinetic full-f particle-in-cell simulations on open field lines with PICLS. *Contributions to Plasma Physics*. 2020;60:e201900117. https://doi.org/10.1002/ctpp.201900117